Revista Mexicana de Astronomía y Astrofísica, **58**, 387–393 (2022)

https://doi.org/10.22201/ia.01851101p.2022.58.02.17

THE PRINCIPAL ASTROPHYSICAL PARAMETERS OF THE OPEN CLUSTERS *GULLIVER* 18 AND *GULLIVER* 58 DETERMINED USING GAIA EDR3 DATA

A. L. Tadross and E. G. Elhosseiny

National Research Institute of Astronomy and Geophysics, Cairo, Egypt.

Received May 19 2022; accepted August 3 2022

ABSTRACT

A photometric and astrometric study of the two open star clusters *Gulliver*18 and *Gulliver*58 was carried out for the first time using the early third data release of the Gaia space observatory (Gaia-EDR3). By studying the proper motions, parallaxes, and color-magnitude diagrams of the two clusters, we determined their actual cluster membership. Therefore, ages, color excesses, and heliocentric distances of the clusters could be determined. The luminosity function, mass function, total mass, mass segregation, and relaxation time of *Gulliver*18 and *Gulliver*58 were estimated as well.

RESUMEN

Se realizó por primera vez un estudio fotométrico y astrométrico de dos cúmulos abiertos, *Gulliver*18 y *Gulliver*58, con los datos preliminares de la tercera entrega del observatorio espacial Gaia (Gaia-EDR3). Estudiando los movimientos propios, las paralajes y los diagramas color-magnitud de ambos cúmulos determinamos la pertenencia de estrellas a ellos. Con estos resultados pudimos encontrar las edades, excesos de color y distancias heliocéntricas de los cúmulos. También estimamos la función de luminosidad, la función de masa, la masa total y la segregación de masas, así como el tiempo de relajamiento para *Gulliver*18 y *Gulliver*58.

Key Words: astronomical data bases: miscellaneous — galaxies: photometry — Hertzsprung-Russell and colour-magnitude — open clusters and associations: individual: Gulliver 18, Gulliver 58

1. INTRODUCTION

This article is part of our series whose goal is to use ideal contemporary datasets to obtain the basic astrophysical properties of poorly studied and/or unstudied open star clusters. Open star clusters (OCs) are important astronomical objects to study the Milky Way structure and evolution. OCs supply useful information about star formation mechanisms, where their main parameters, i.e., age, distance, and reddening can be derived directly from their color-magnitude diagrams (CMDs). This can be accurately achieved when we first determine the actual membership of the clusters under study (Barnes 2007; Perren et al. 2015; Sariya et al. 2017; Marino et al. 2018).

From SIMBAD (`http://simbad.cds.unistra.fr/simbad/sim-fbasic`), we obtained the cluster centers in equatorial and Galactic coordinates. Gulliver 18 (hereafter G18) is located at (α = 20h 11m 37s, $\delta = +26^\circ\,31'\,55''$, $l = 65.526^\circ$, $b = -3.97045^\circ$, $J2000$) in the Vulpecula constellation, whereas Gulliver 58 (hereafter G58) is located at (α = 12h 46m 4s, $\delta = -61^\circ\,57'\,54''$, $l = 302.3^\circ$, $b = 0.9^\circ$, $J2000$) in the Centaurus constellation. Figure 1 shows the negative images of G18 and G58 as taken from ALADIN at DSS-colored optical wavelengths. Cantat-Gaudin et al. (2018) studied the main astrometric parameters of those two clusters, i.e., coordinates, proper motions, parallaxes, and distances as newly discovered clusters in the Milky-Way Galaxy. They used the second data release of the Gaia DR2 database, Gaia Collaboration et al. (2018).

Here, we estimate the fundamental parameters of the two clusters G18 and G58 for the firs time using the early third release of the Gaia database (Gaia EDR3) - Gaia Collaboration et al. (2021), which was

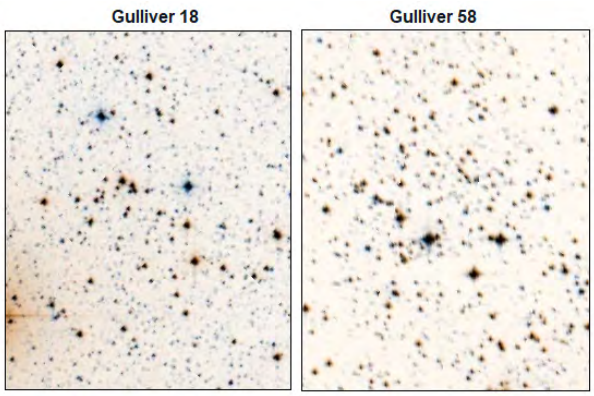

Fig. 1. Inverse colored (negative) images of the clusters $G18$ and $G58$ as taken from ALADIN at DSS colored optical wavelength. These two clusters lie in the Vulpecula and Centaurus constellations, respectively. North is up and East to the left. The color figure can be viewed online.

published on December 3, 2020. Gaia EDR3 offers improved astrometry and photometry for 1.8 billion sources brighter than $G \approx 21$ mag. Compared to Gaia DR2, the parallax enhancement is 20% and the proper motions are twice more accurate. The most important part of using the Gaia EDR3 involves five astrometric parameters: equatorial positions (α, δ), proper motions $(\mu\alpha \cos\delta,\ \mu\delta)$, and parallaxes $(\bar{\omega})$. In addition, the magnitudes in three photometric filters (G, G_{BP}, G_{RP}) were obtained with better homogeneity due to the significant advance in several aspects (Gaia Collaboration et al. 2021; Torra et al. 2021; Riello et al. 2021). Of course, all of these improvements affect the astrophysical estimated parameters of the clusters under study.

The paper is organized as follows: the Gaia EDR3 dataset and membership determination are presented in § 2. § 3 shows the angular size according to the radial density profiles (RDPs). § 4 contains the photometry of the color-magnitude diagrams (CMDs). § 5 describes the clusters' dynamic states, i.e., luminosity functions (LFs), mass functions (MFs), mass segregation and relaxation times. § 6 summarizes the results and presents the conclusions.

2. GAIA EDR3 DATASET AND MEMBERSHIP

The standard dataset of G18 and G58 was downloaded from the Gaia EDR3 I/350 Vizier catalog website. A circular region of 20 arcmin radius centered in the celestial position was applied to each cluster. The error ranges of the parallaxes are up to 0.03 mas for $G < 15$ mag, 0.07 mas for $G \approx 17$ mag, 0.5 mas for $G \approx 20$ mag, and 1.3 mas for $G \approx 21$ mag. The error ranges of the proper motions (PMs) are up to 0.03 mas/yr for $G < 15$ mag, 0.07 mas/yr for $G \approx 17$ mag, 0.5 mas/yr for $G \approx 20$ mag, and 1.4 mas/yr for $G \approx 21$ mag.

Using high-precision Gaia EDR3 parallaxes and proper motions, we can easily remove the background field stars from the cluster's main sequence (Bellini et al. 2009; Yadav et al. 2013; Sariya & Yadav 2015; Tadross 2018). The vector point diagrams (VPDs), $\mu\alpha \cos\delta$ vs $\mu\delta$ of $G18$ and $G58$ are shown in Figure 2. The greatest density area (the darkest spot) is taken as the subset of the cluster's most likely members (Tadross 2018; Tadross & Hendy 2021, 2022).

In our analysis, we used the software named TOPCAT. This is a tool that can handle huge and sparse datasets. It was initially created for astronomy to support virtual observatories. The acronym TOPCAT derives from Tool for OPerations on Catalogues And Tables. It can support several digital file formats, including FITS, which is widely used in astronomy (`http://www.star.bris.ac.uk/~mbt/topcat/`).

Within the subset of the cluster's most likely members, only those stars with magnitudes $G \leq 20.5$, located inside the cluster's estimated size (see § 3) were taken into account. Mean values and standard deviations of the parallax and the two components of the proper motions were calculated for all these stars (excluding negative values of the parallax, see the lower right-hand panel of Figure 4). Stars are then considered to be cluster members only if their 3σ parallax and proper motion errors lie within the cluster's mean values with respect to the background field ones. According to Lindegren et al. (2018), all the parallax values should be shifted by adding 0.029 mas to their values. In addition, the value of the renormalized unit weight error, RUWE, indicates how well the source matches the single-star model - it should be less than 1.4.

Using TopCat, we can identify comoving stars, i.e., those stars that move at the same speed and direction in the sky, as shown in Figure 3. It is worth noting that the selected subset of VPDs influences the CMDs and field star separation. The CMDs of the clusters appear cleaner when those conditions are applied (Anderson et al. 2006; Sariya et al. 2017).

3. ANGULAR SIZE

The boundary and core radii of $G18$ and $G58$ were calculated using King (1966) radial density profile (RDP). To do so, we built a series of concentric circles centered on the clusters' central coordinates.

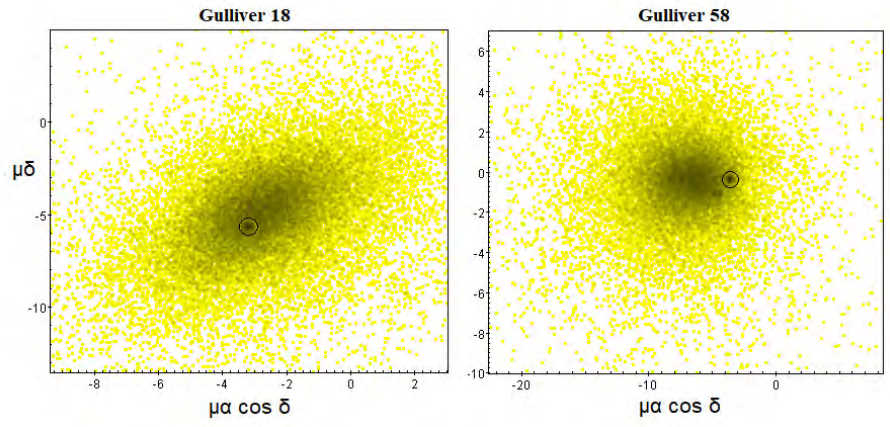

Fig. 2. The vector point diagrams of the clusters G18 and G58. The circles denote the darkest areas, in which the subsets of the most likely members lie. The color figure can be viewed online.

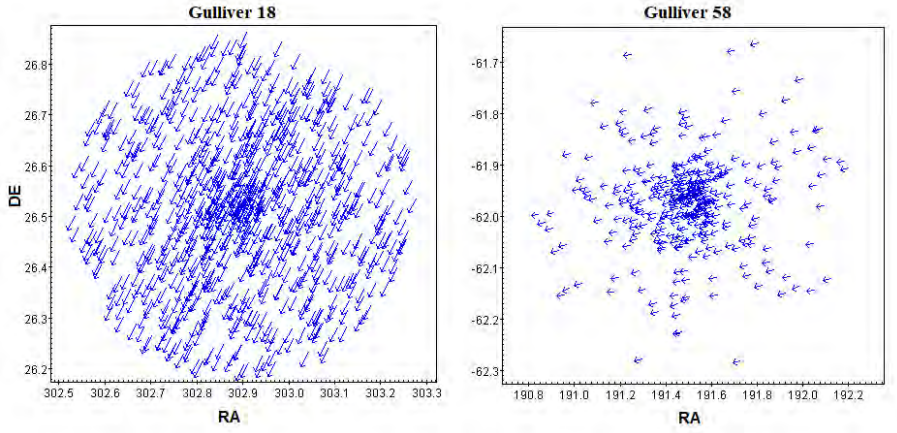

Fig. 3. Comoving stars of clusters G18 and G58. They are the stars included in the subsets we selected in the VPDs, i.e., the stars that move at the same speed and direction in the sky. The color figure can be viewed online.

The number of stars found in each ring was divided by the ring area to obtain the stellar density $f(R)$. The upper right-hand panel of Figure 4 shows the measured star density vs. the distance to the cluster center. The King model fit can be given by the equation:

$$f(R) = f_{bg} + \frac{f_0}{1 + (\frac{R}{R_c})^2}, \quad (1)$$

where R is the radius from the cluster center, f_0 the central density, R_c the core radius and f_{bg} the background density. We can find these parameters from the King model as follows:

	R_c	f_{bg}	f_0
$G18$	0.35	50	233
$G58$	0.27	33	305

When the stars approach the boundary radius, they begin to dissolve within the background density. Knowing the previous parameters, we can get the boundary radius by applying the equation of Bukowiecki et al. (2011) as follows:

$$R = R_c \sqrt{\frac{f_0}{3\sigma_{bg}} - 1}, \quad (2)$$

where σ_{bg} is the uncertainty of f_{bg}. Consequently, the estimated boundary radii of $G18$ and $G58$ are found to be 7.5 ± 0.5 arcmin (3.0 pc) and 4.5 ± 0.3 arcmin (1.9 pc), respectively.

On the other hand, the tidal radius of a cluster is defined as the distance from the cluster core at which the Galaxy's gravitational influence equals that of the cluster core. Estimating the total masses of $G18$ and $G58$ (see § 5), the tidal radius can be calculated

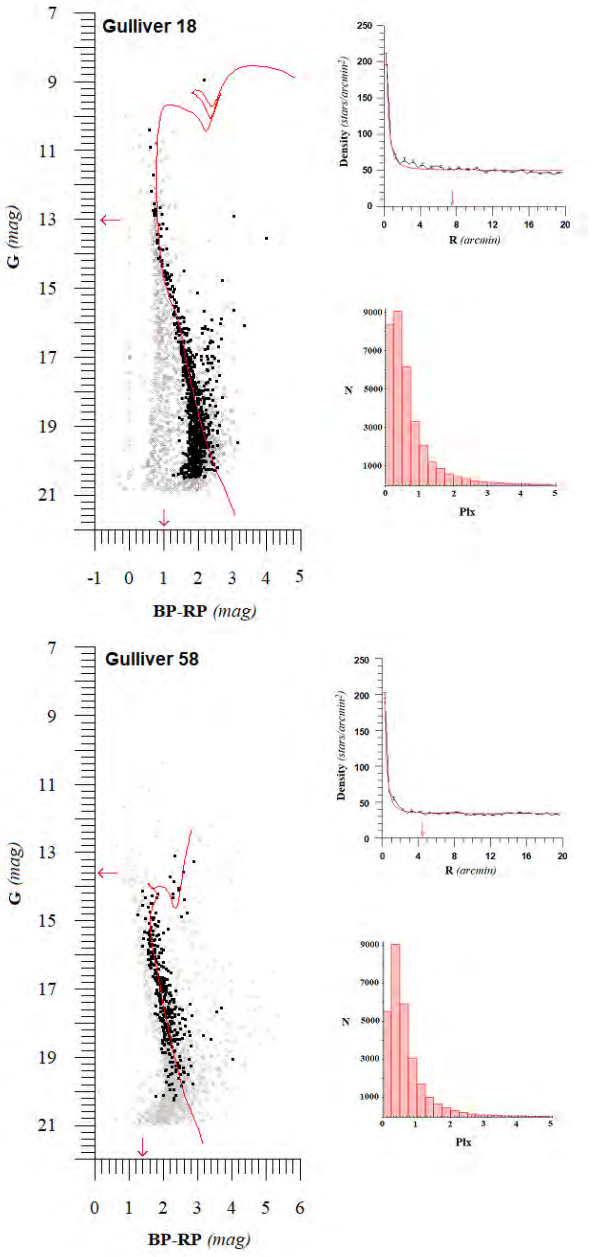

Fig. 4. The left-hand panels show the main sequence curves of $G18$ and $G58$ fitted to the solar metallicity theoretical isochrones of Padova. The ages are found to be 100 ± 10 Myr and 1.0 ± 0.1 Gyr, respectively. The distance moduli and color excesses are found to be $12.3, 13.6\,(\pm 0.25)$ mag, 0.8 and $1.4\,(\pm 0.10)$ mag, respectively. The right-hand panels show the radial density profiles fitted to the King (1966) model and the histograms of parallaxes of the selected stars ($\bar{\omega} > 0$). The estimated radii of $G18$ and $G58$ are found to be 7.5 and $4.5\,(\pm 0.50)$ arcmin and the mean values of the parallaxes are found to be 0.50 and $0.45\,(\pm 0.05)$ mas, respectively. The color figure can be viewed online.

using the form of Jeffries et al. (2001) as follows:

$$R_t = 1.46 \times M_c^{\frac{1}{3}}, \tag{3}$$

where R_t is the tidal radius (in parsec) and M_c the total mass of the cluster (in solar masses). The tidal radii of $G18$ and $G58$ are found to be 17.8 and $11.0\,(\pm 0.2)$ pc, respectively. The concentration parameter of Peterson & King (1975), $C = \log(\frac{R}{R_c})$, shows us whether the cluster is prominent or condensed with respect to the background field stars. We found that both clusters are insufficiently condensed objects.

4. CMD PHOTOMETRY

The study of CMD is a widely used technique to characterize the observed main sequence of the cluster. This is achieved by finding the best fit of one of the Padova PARSEC databases of stellar evolutionary isochrones (`http://stev.oapd.inaf.it/cgi-bin/cmd`) of Bressan et al. (2012) to the observed main-sequence curve of the cluster. To decrease the effect of field stars contamination, only the most likely cluster members are taken into account. Since the cluster members have a common origin, they share the same speed and direction in the sky. This fact makes proper motions a valuable tool for removing nonmember stars from each cluster's main sequence (Yadav et al. 2013; Bisht et al. 2020).

Based on the CMDs of $G18$ and $G58$, as shown in the left-hand panel of Figure 4, only the stars within the cluster's boundary size and parallaxes ranges are represented. The mean values of the parallaxes are found to be 0.50 and $0.45\,(\pm 0.05)$ mas, respectively. Clusters fittings were quite good by shifting the isochrones of ages 100 ± 10 Myr and 1.0 ± 0.1 Gyr with apparent distance moduli $(m-M)$ of 12.3 and $13.6\,(\pm 0.25)$ mag, respectively. In addition, the color excesses $E(BP-RP)$ are found to be 0.8 and $1.4\,(\pm 0.10)$ mag, respectively. Note that $G18$ and $G58$ are close to areas with a lot of dust with high differential extinction in their fields along their lines of sight, as displayed in the 3D extinction map (`http://argonaut.skymaps.info`).

Reddening is a critical parameter affecting the total absorption value that must be subtracted from the apparent distance modulus to obtain the true distance to the cluster. We used the Padova PARSEC database of stellar evolutionary tracks and isochrones, which is scaled to the solar metallicity of 0.0152. The Gaia filter passbands are taken from Riello et al. (2021), where $A_G/A_\nu = 0.836$, $A_{GBP}/A_\nu = 1.083$, and $A_{GRP}/A_\nu = 0.634$. These

TABLE 1

THE PRINCIPAL ASTROPHYSICAL PARAMETERS OF $G18$ AND $G58$*

Parameter	Gulliver 18	Gulliver 58
RA (h: m: s)	20:11:37	12:46:04
DE (°: ′ : ″)	+26:31:55	-61:57:54
G. long. (°)	65.526	302.30
G. lat. (°)	-3.97	0.90
Age (Myr)	100 ± 10	1000 ± 100
Radius (arcmin)	7.5 ± 0.5	4.5 ± 0.3
Core Radius (arcmin)	0.35 ± 0.07	0.27 ± 0.04
Tidal Radius (pc)	17.8 ± 0.5	11.0 ± 0.5
m-M (mag)	12.3 ± 0.25	13.6 ± 0.25
E(BP-RP) (mag)	0.8 ± 0.1	1.4 ± 0.1
E(B-V) (mag)	0.61 ± 0.1	1.06 ± 0.1
Dist. (pc)	1370 ± 65 (1558.6)	1425 ± 65 (2344.2)
Relax. Time (Myr)	31.5 ± 5	9.5 ± 5
P.M. (mas/sec)	6.515 ± 0.45 (6.488)	3.652 ± 0.35 (3.609)
Plx. (mas)	0.50 ± 0.07 (0.613)	0.45 ± 0.07 (0.398)
Rgc (kpc)	6.75 ± 0.2	6.55 ± 0.2
$X_\odot$ (pc)	-565 ± 40	-760 ± 60
$Y_\odot$ (pc)	1241 ± 55	-1201 ± 50
$Z_\odot$ (pc)	-95 ± 5	22 ± 5

*The values in brackets are the corresponding astrometric measurements obtained by Cantat-Gaudin et al. (2018).

ratios have been used for correction of the magnitudes for the interstellar reddening and for converting the color excess to $E(B-V)$, where $R_v = A_\nu/E(B-V) = 3.1$. Therefore, we can estimate the true distance moduli $(m-M)_0$ of $G18$ and $G58$, from which we infer heliocentric distances of 1370 and 1425 (±65) pc, respectively. Correspondingly, the Cartesian Galactocentric coordinates $(X_\odot; Y_\odot; Z_\odot)$ and the distances from the Galactic center (R_g) are estimated for the two clusters as listed in Table 1. According to our calculations mentioned in Tadross (2011), the $Y-$axis connects the Sun to the Galactic center, being positive to the Galactic anticenter, while the $X-$axis is perpendicular to $Y-$axis, being positive in the first and second Galactic quadrants (Lynga 1982). We adopted a Galactocentric distance (R_g) of 7.2 kpc (Bica et al. 2006).

5. THE DYNAMIC STATE OF THE CLUSTERS

5.1. *Luminosity and Mass Functions*

We used the photometric dataset of Gaia EDR3 to derive the clusters' luminosity functions (LFs) and mass functions (MFs). The LF represents the distribution of the absolute magnitudes of the cluster's members. Using the distance moduli obtained from the isochrone fittings, we transformed the apparent G magnitudes of the cluster members into absolute magnitudes. Then, the LF diagrams can be constructed as shown in the upper panel of Figure 5. Note that the LFs increase up to $M_G \approx 8.15$ and 4.20 mag for $G18$ and $G58$, respectively.

The initial mass function (IMF) provides the main bond between the bright massive members and less massive fainter ones. It is a historic record of the star formation process and plays the main role in understanding the early dynamic development of star clusters. The IMF was estimated for the bright massive stars ($\geq 1M_\odot$) by Salpeter's (1955) power law, where the number of stars in each mass range decreases as the mass increases. It can be written as follows:

$$\log \frac{dN}{dM} = -(1+x)\log(M) + const., \qquad (4)$$

where dN is the number of stars in a mass bin dM with a central mass M and x is the MF slope. To convert LF into MF, we used the last version of the theoretical isochrones of Padova's stellar evolutionary tracks and isochrones. The resulting mass functions of $G18$ and $G58$ are shown in the lower panel of Figure 5. The derived values of the MF slope are

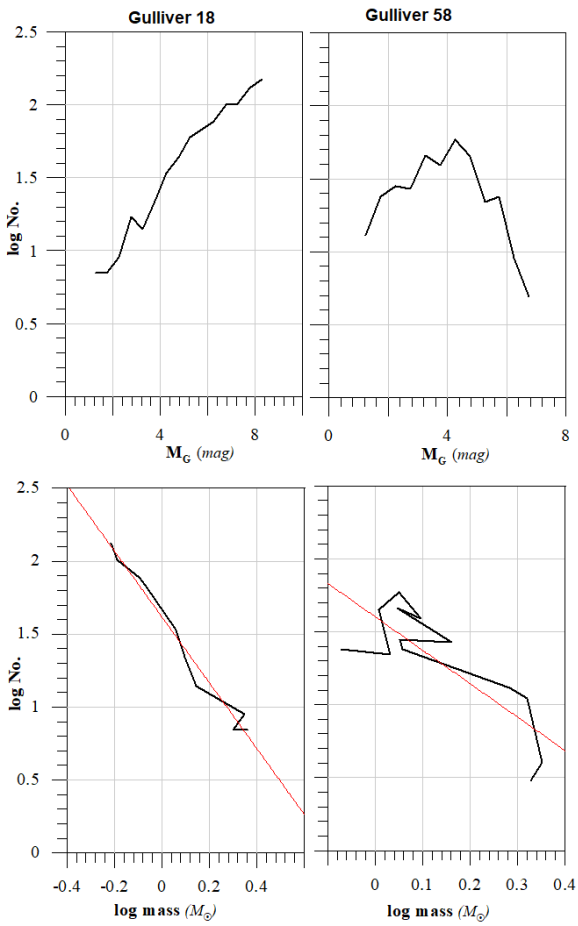

Fig. 5. The upper panel represents the luminosity functions of $G18$ and $G58$. Note that the LFs increase up to $M_G \sim 8.15$ and 4.20 mag for $G18$ and $G58$, respectively. The lower panel represents the mass distribution of the two clusters. The red lines show the linear fittings of the mass functions' slopes, which are found to be 2.25 and 2.29 ($\pm$ 0.15) for $G18$ and $G58$, respectively. The color figure can be viewed online.

found to be $x = 2.25$ and 2.29 ($\pm$ 0.15) for $G18$ and $G58$, respectively, which agree with Salpeter's mean value.

5.2. *Mass Segregation*

Mass segregation in a real cluster implies that the massive stars are more concentrated toward the cluster center than less massive stars. Mass segregation is a result of the dynamic evolution of the cluster and/or an impression of star construction processes themselves, or both (Sagar 2002). To explore if there is actual mass segregation, we divided the clusters' stars into four bands, G<17 ; 17≤G≤18; 18≤G≤19 and G≥19 mag. Drawing these bands as a function

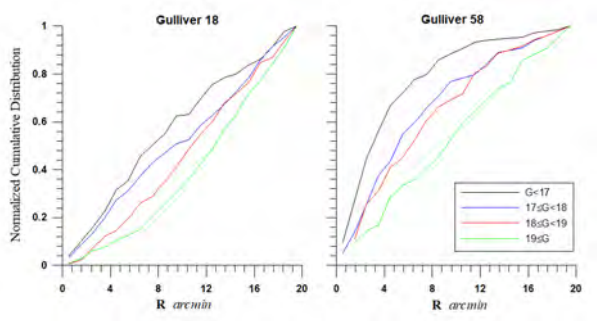

Fig. 6. The cumulative frequency distributions of $G18$ and $G58$ represent the radial distance and magnitude distributions of the clusters' member bands (mass segregation). The bright, massive stars are more likely to settle toward the clusters' centers than the fainter, less massive, ones. The color figure can be viewed online.

of the distances from the cluster's center as shown in Figure 6, we found that the bright massive stars are more likely to settle toward the cluster center than the less massive fainter ones.

5.3. *Relaxation Time*

Once the distribution of the cluster members' velocities becomes almost Maxwellian, a metric for understanding the dynamical evolution is considered. This period is known as "relaxation time" (T_R) and can be defined by the equation of Spitzer & Hart (1971) as follows:

$$T_R = \frac{8.9 \times 10^5 \sqrt{N} \times R_h^{1.5}}{\sqrt{\langle m \rangle} \times \log(0.4N)}, \qquad (5)$$

where N is the number of cluster members, R_h is the cluster's radius that contains half of the cluster's total mass (in pc) and $\langle m \rangle$ is the average mass of a member star (in solar masses). Thus, the dynamic relaxation times are found to be 31.5 and 9.5 ($\pm$ 5.0) Myr for $G18$ and $G58$, respectively. The clusters under investigation are thus found to be older than their estimated relaxation times. We conclude that $G18$ and $G58$ are dynamically relaxed clusters.

6. RESULTS AND CONCLUSIONS

The principal properties of the two open clusters Gulliver 18 and Gulliver 58 were looked into in this paper for the first time using the Gaia EDR3 database. Both clusters are located in the Vulpecula and Centaurus constellations, respectively; they are not sufficiently condensed objects in the sky. The MF slopes of $G18$ and $G58$ are found to agree with

Salpeter's (1955) mean value. The two clusters are dynamically relaxed as their estimated relaxation times are much smaller than their ages. Table 1 summarizes the main results of our study.

This work is a part of the project named (IMHOTEP) No. 42088ZK between Egypt and France. It was begun in 2019 and finished in 2021. Many thanks to Prof. David Valls-Gabaud (Paris Observatory) for being a companion in that project. This work has made use of data from the European Space Agency (ESA) mission Gaia processed by the Gaia Data Processing and Analysis Consortium (DPAC), (https://www.cosmos.esa.int/web/gaia/dpac/consortium). Funding for the DPAC has been provided by national institutions, in particular, the institutions participating in the Gaia Multilateral Agreement (MLA). The Gaia mission website is https://www.cosmos.esa.int/gaia. The Gaia archive website is https://archives.esac.esa.int/gaia.

REFERENCES

Anderson, J., Bedin, L. R., Piotto, G., et al. 2006, A&A, 454, 1029, https://doi.org/10.1051/0004-6361:20065004

Barnes, S. A. 2007, ApJ, 669, 1167, https://doi.org/10.1086/519295

Bellini, A., Piotto, G., Bedin, L. R., et al. 2009, A&A, 493, 959, https://doi.org/10.1051/0004-6361:200810880

Bica, E., Bonatto, C., Barbuy, B., & Ortolani, S. 2006, A&A, 450, 105, https://doi.org/10.1051/0004-6361:20054351

Bisht, D., Zhu, Q., Yadav, R. K. S., Durgapal, A., & Rangwal, G. 2020, MNRAS, 494, 607, https://doi.org/10.1093/mnras/staa656

Bressan, A., Marigo, P., Girardi, L., et al. 2012, MNRAS, 427, 127, https://doi.org/10.1111/j.1365-2966.2012.21948.x

Bukowiecki, Ł., Maciejewski, G., Konorski, P., & Strobel, A. 2011, AcA, 61, 231

Cantat-Gaudin, T., Jordi, C., Vallenari, A., et al. 2018, A&A, 618, 93, https://doi.org/10.1051/0004-6361/201833476

Gaia Collaboration, Brown, A. G. A., Vallenari, A., et al. 2018, A&A, 616, 1, https://doi.org/10.1051/0004-6361/201833051

Gaia Collaboration, Brown, A. G. A., Vallenari, A., et al. 2021, A&A, 649, 1, https://doi.org/10.1051/0004-6361/202039657

Jeffries, R. D., Thurston, M. R., & Hambly, N. C. 2001, A&A, 375, 863, https://doi.org/10.1051/0004-6361:20010918

King, I. R. 1966, AJ, 71, 64, https://doi.org/10.1086/109857

Lindegren, L., Hernández, J., Bombrun, A., et al. 2018, A&A, 616, 2, https://doi.org/10.1051/0004-6361/201832727

Lynga, G. 1982, A&A, 109, 213

Marino, A. F., Milone, A. P., Casagrande, L., et al. 2018, ApJ, 863, 33, https://doi.org/10.3847/2041-8213/aad868

Perren, G. I., Vázquez, R. A., & Piatti, A. E. 2015, A&A, 576, 6, https://doi.org/10.1051/0004-6361/201424946

Peterson, C. J. & King, I. R. 1975, AJ, 80, 427, https://doi.org/10.1086/111759

Riello, M., De Angeli, F., Evans, D. W., et al. 2021, A&A, 649, 3, https://doi.org/10.1051/0004-6361/202039587

Sagar, R. 2002, IAUS 207, Extragalactic Star Clusters, ed. D. Geisler, E. K. Grebel, & D. Minniti (San Francisco, CA: ASP), 515

Salpeter, E. E. 1955, ApJ, 121, 161, https://doi.org/10.1086/145971

Sariya, D. P., Jiang, I.-G., & Yadav, R. K. S. 2017, AJ, 153, 134, https://doi.org/10.3847/1538-3881/aa5be6

Sariya, D. P. & Yadav, R. K. S. 2015, A&A, 584, 59, https://doi.org/10.1051/0004-6361/201526688

Spitzer, L. Jr. & Hart, M. H. 1971, ApJ, 166, 483, https://doi.org/10.1086/150977

Tadross, A. L. 2011, JKAS, 44, 1, https://doi.org/10.5303/JKAS.2011.44.1.1

_____. 2018, RAA, 18, 158, https://doi.org/10.1088/1674-4527/18/12/158

Tadross, A. L. & Hendy, Y. H. 2021, ApJ, 42, 6, https://doi.org/10.1007/s12036-020-09648-5

_____. 2022, AdSpR, 69, 467, https://doi.org/10.1016/j.asr.2021.09.014

Torra, F., Castañeda, J., Fabricius, C., et al. 2021, A&A, 649, 10, https://doi.org/10.1051/0004-6361/202039637

Yadav, R. K. S., Sariya, D. P., & Sagar, R. 2013, MNRAS, 430, 3350, https://doi.org/10.1093/mnras/stt136

Ashraf L. Tadross and Eslam G. Elhosseiny: National Research Institute of Astronomy and Geophysics, Cairo, Egypt, EL Marsad Street 1, Helwan, Cairo, Egypt (altadross@nriag.sci.eg), (eslam_elhosseiny@nriag.sci.eg).